JOURNAL OF Materials CHEMISTRY

New electron-transporting materials for light emitting diodes: 1,3,4-oxadiazole–pyridine and 1,3,4-oxadiazole–pyrimidine hybrids

Changsheng Wang,[a] Gun-Young Jung,[b] Andrei S. Batsanov,[a] Martin R. Bryce*[a] and Michael C. Petty*[b]

[a]*Department of Chemistry, University of Durham, South Road, Durham, UK DH1 3LE. Fax: 44-191-384-4737; E-mail: m.r.bryce@durham.ac.uk*
[b]*School of Engineering, University of Durham, South Road, Durham, UK DH1 3LE*

Received 30th July 2001, Accepted 7th November 2001
First published as an Advance Article on the web 17th December 2001

We describe the synthesis of three new isomeric 1,3,4-oxadiazole–pyridine hybrids, namely: 2,6-, 3,5- and 2,4-bis[2-(4-*tert*-butylphenyl)-1,3,4-oxadiazol-5-yl]pyridine, (PDPy-2,6, PDPy-3,5 and PDPy-2,4, respectively) and a 1,3,4-oxadiazole–pyrimidine hybrid, namely: 2,5-bis[2-(4-*tert*-butylphenyl)-1,3,4-oxadiazol-5-yl]pyrimidine (PDPmDP). The X-ray crystal structures are reported for PDPy-2,4 and the known phenylene analogue 1,3-bis[2-(4-*tert*-butylphenyl)-1,3,4-oxadiazol-5-yl]benzene (OXD-7) as a 1 : 1 toluene solvate. The packing motif for molecules of both PDPy-2,4 and OXD-7 is that of discrete layers with the mean planes of all the molecules in the crystals parallel to within 6°. We have fabricated light-emitting diodes (LEDs) using poly[2-methoxy-5-(2-ethylhexyloxy)-1,4-phenylenevinylene] (MEH-PPV) doped with rubrene as the emissive material, with and without a thermally evaporated electron conducting/hole-blocking (ECHB) layer of PDPy-2,6, PDPy-3,5 and PDPy-2,4, PDPmDP and OXD-7, in the device configuration ITO/MEH-PPV(Ru)/ECHB layer/Al. Electroluminescence spectra indicate that light is emitted only from the MEH-PPV layer. The bilayer LEDs are considerably more efficient than single layer devices, *e.g.* the external quantum efficiences of devices incorporating PDPy-2,6, PDPy-3,5 and OXD-7 are 0.14, 0.04 and 0.06% at 40 mA m^{-2}, respectively, *cf.* 0.007% for the reference single-layer MEH-PPV(Ru) device. There is no clear correlation between experimental EQE values and the PM3 calculated LUMO levels of the materials.

Introduction

During the past ten years research in the field of organic light-emitting diodes (LEDs) based on electroluminescence of conjugated polymers has flourished due to their potential applications in display technologies.[1] An optimised LED requires efficient and balanced charge injection from both electrodes, comparable transporting properties of both holes and electrons, a high external quantum efficiency and a long lifetime for the device. In this context, 2,5-diaryl-1,3,4-oxadiazole derivatives have enjoyed widespread use as electron-transporting/hole blocking (ECHB) materials in multilayer devices, due to the electron-deficient nature of this heterocycle, high photoluminescence quantum yield and the good thermal and chemical stabilities of the materials.[2] Examples include molecular systems[3] and polymers[4] in which the oxadiazole unit is incorporated into the main chain or as a pendant substituent.

Pyridine is also an electron-deficient heterocycle, and it has been established that the introduction of pyridine units into the main chain of conjugated *p*-phenylene and 9,9-dialkylfluorene type polymers improves the electron-transporting properties of these materials.[5] In the light of these precedents we combined 1,3,4-oxadiazole and pyridine units in the same molecule and recently reported the ECHB properties of the first system of this type, *viz.* PDPyDP (**2d**, Scheme 1).[6] LEDs were fabricated using poly[2-methoxy-5-(2′-ethylhexyloxy)-*p*-phenylenevinylene] (MEH-PPV) as the emissive layer with and without a thermally evaporated layer of compounds **2a**, **2b** or **2d** as an ECHB layer. Using aluminium as the cathode the bilayer device with compound **2d** was found to be considerably more efficient than the corresponding single layer device, or devices with **2a** or **2b** as the ECHB layer.[6] We also found that the bilayer LED with **2d** as the ECHB layer was initially unstable to ambient conditions. However, we showed that by thermal annealing of the degraded device, or increasing the deposition rate and thickness of the thermally evaporated Al cathode, the stability/operating lifetime of the bilayer device with compound **2d** was significantly improved.[7b]

We also noted recently that the two geometrical isomers, namely, PDPDP (**2b**) and OXD-7 (**2c**) had different electron-injectabilities in bilayer LEDs using MEH-PPV as the emissive material.[8] This suggested that the geometrical isomers of PDPyDP (**2d**) should also be examined. Therefore, compounds **2e–g**, the angular 2,6-, 3,5- and 2,4-isomers, respectively, of the linear 2,5-isomer **2d** have been synthesised. We explained the improved electron-injecting performance of PDPyDP (**2d**) over its phenylene analogues PDPDP (**2b**) and OXD-7 (**2c**), on the basis of increased electron deficiency arising from the more electronegative nitrogen atom in the pyridine unit.[6] Following this premise, PDPmDP (**2h**) was designed as an analogue of **2d**, with an additional nitrogen atom introduced into the central conjoining ring. We also report the synthesis of this new molecule and its applications as an ECHB layer in LEDs based on MEH-PPV.

Results and discussion

Synthesis

The synthesis of the three angular pyridine derivatives **2e–g** (Scheme 1) was based on our reported route to PDPyDP (**2d**).[6] However, the synthesis of the pyrimidine analogue PDPmDP (**2h**) was not so straightforward due to the difficulties in obtaining the key starting material 2,5-pyrimidine dicarboxylic acid (**4**). Our recent success in synthesising another difficult

DOI: 10.1039/b106907c

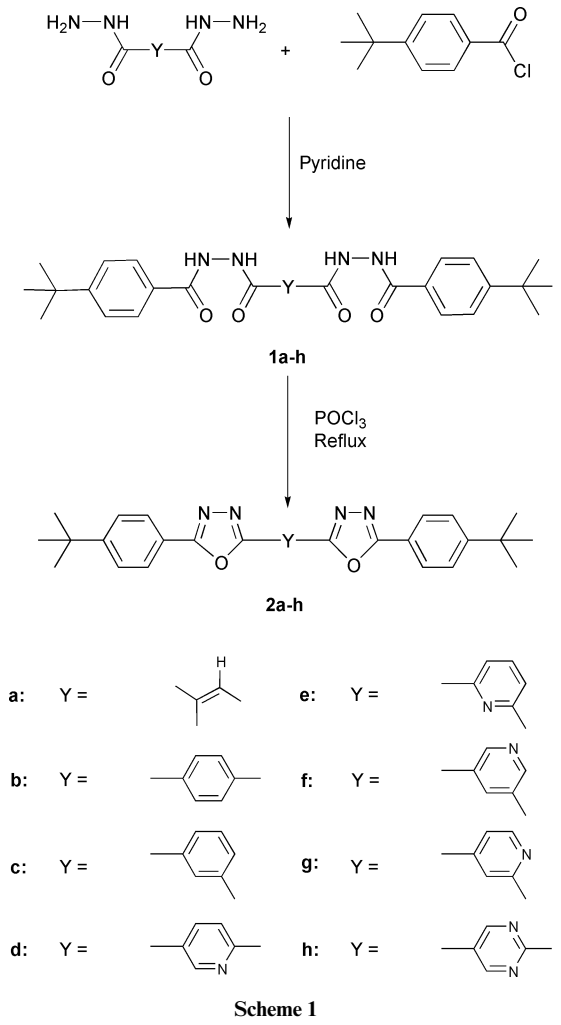

Scheme 1

carboxylic acid, 5-bromo-2-pyridinecarboxylic acid,[4e] encouraged us to apply the same methodology to 2,5-dibromopyrimidine,[9] and the method has proved to be an efficient and economical way of preparing this diacid **4** (Scheme 2). Treating dibromopyrimidine with 2-methylbut-3-yn-2-ol (which costs only GBP11.50/500 cm^3 from Lancaster) in the presence of CuI, $Pd(PPh_3)_2Cl_2$ (2%) and triethylamine afforded the diethynylpyrimidine derivative **3** in good yield. Compound **3** can be easily purified by recrystallisation from toluene.

A classical oxidation of compound **3** with $KMnO_4$ in aqueous phase in the presence of Aliquat-336 as reported for a methylpyridine oxidation[10] gave the pyrimidinedicarboxylic acid **4** in good yield. The structure was unambiguously characterised by derivatising it to its diethyl ester **5**. It is worth noting that the diacid **4** has been reported once, obtained by oxidation of 2-methylquinazoline, with a melting point of 278–280 °C.[11] However, we failed to observe a melting process at temperatures below 330 °C for our solids. Taking advantage of this new and convenient route to the diethyl ester **5**, we had little difficulty in synthesising the pyrimidine–oxadiazole hybrid **2h** *via* the subsequent reactions shown in Scheme 1.

UV-Vis absorption spectra of compounds 2d–h

The solution UV-Vis absorption spectra of compounds **2b–h** can be roughly divided into the angular group (**2c**, **2e–g**) and the linear group (**2b**, **2d**, **2h**) (Fig. 1). The absorptions of the low energy $^1(\pi-\pi^*)$ transitions of the former group have similar shapes centred at *ca.* 300 nm. They all show three overlapping features within this band, but the relative oscillator strength of each feature varies as the position of the nitrogen atom in the pyridine ring changes, causing the shifts of the absorption maxima. Among these four angular compounds, the absorption profiles of OXD-7 (**2c**) and PDPy-3,5 (**2f**) have almost identical shapes with absorption maxima at 292 and 297 nm, respectively, indicating that replacing a CH group with a N atom leads to a red-shift, although this replacement causes no relief of steric hindrance. Semi-empirical (PM3)[12] calculations also show that **2f** had a reduced LUMO (lowest unoccupied molecular orbital)–HOMO (highest occupied molecular orbital) band gap compared to **2c** (Table 1), indicating that the reduced band gap and hence the red-shift of the absorption are due to the nitrogen atom.

The absorption profiles of the three linear molecules (**2b**, **2d**, **2h**) also have almost the same features. As seen for **2c** and **2f**, the λ_{max} values red shift as the number of nitrogen atoms in the central conjoining ring increases. The red-shifts of these three compounds could be explained by 1) the increased planarity due to the reduced steric hindrance between the central conjoining ring and the neighbouring oxadiazole ring; 2) nitrogen electronic effects as was suggested by **2c** and **2f**, by replacing the C–H groups with N-atoms.

Our recent studies indicate that protonation of conjugated

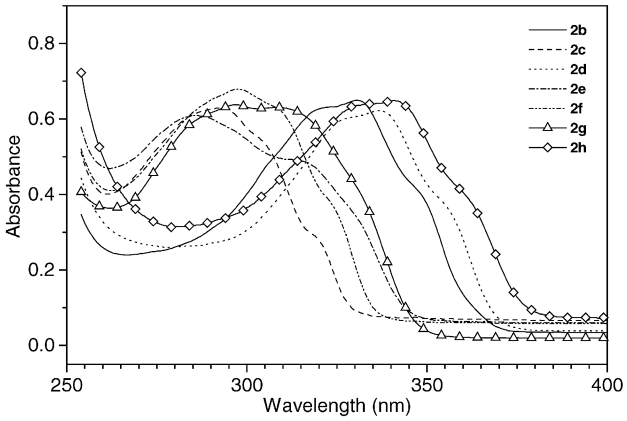

Fig. 1 UV-VIS absorption spectra of compounds **2b–h** in chloroform solution.

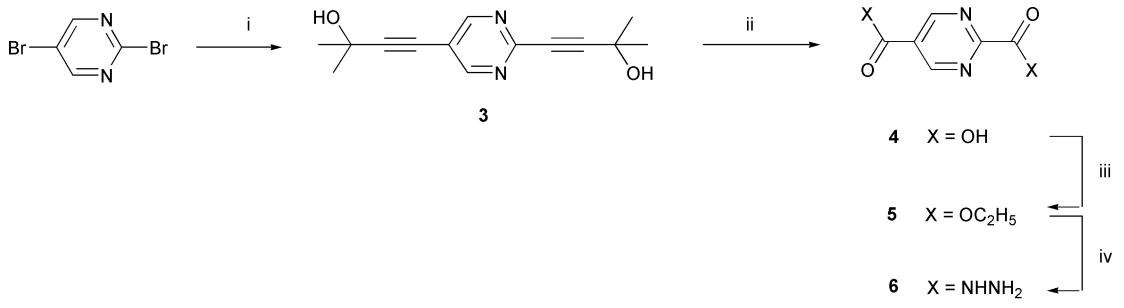

Scheme 2 *Reagents and conditions*: i, 2-methylbut-3-yn-2-ol, CuI, $Pd(PPh_3)_2Cl_2$, triethylamine, THF, 20 °C, 1 h, then reflux 1 h; ii, $KMnO_4$, Aliquat-336, H_2O, 100 °C; iii, $SOCl_2$, reflux 4 h, then EtOH, pyridine, reflux 12 h; iv, hydrazine monohydrate, EtOH, reflux 2 h.

Table 1 UV-Vis absorption maxima, PM3 calculated energy levels and net-charges on the pyridine (pyrimidine for **2h**) N atoms

Compound	λ_{max}/nm	HOMO/eV	LUMO/eV	ΔE/eV	Net Charge of N in Py	E.Q.E (%) at 40 mA cm^{-2}
2b	331	9.03	1.50	7.53		0.11
2c	292	9.13	1.27	7.86		0.06
2d	337	9.14	1.69	7.45	−0.05	0.14
2d-H$^+$	384	11.62	5.85	5.77	+0.54	
2e	286	9.31	1.27	8.04	−0.02	0.14
2f	298	9.25	1.49	7.76	−0.08	0.04
2f-H$^+$	331	11.67	5.57	6.10	+0.59	
2g	297, 308	9.21	1.49	7.72	−0.04	0.05
2g-H$^+$	380	11.66	5.88	5.78	+0.49	
2h	341	9.24	1.91	7.33	−0.06, −0.09	0.12

pyridine polymers/oligomers can lead to co-planarisation by intramolecular hydrogen-bonding of the two neighbouring rings *via* the proton attached to the nitrogen atom of the pyridine.[13] In this context, we recorded the solution UV-Vis spectra of compounds **2d–h** with and without bubbling HCl gas through the solution. We found that absorptions of **2f** and **2g** were significantly red-shifted by 33 nm and 72 nm, correspondingly, due to protonation (Fig. 2). A similarly red-shifted peak (by *ca.* 47 nm) was also found in the spectrum of the solution of protonated **2d**. However, HCl had virtually no effect on the absorption spectra of compounds **2e** and **2h**. For the case of **2e**, we reasoned that the two strongly electron-withdrawing oxadiazole rings at the *ortho*- positions of the central pyridine ring reduce the electron density on the pyridine-nitrogen atom to a degree that the molecule loses its basicity. Whereas in **2d** (one *ortho*- and one *meta*-) and **2f** (both *meta*-), the electronic effect of oxadiazole is less pronounced. In **2g**, one oxadiazole is at the *ortho*- while the other at the *para*- position. The weaker inductive effect of the *para*-substitution compared with the *ortho*- one also makes **2g** a stronger base than **2e**, which bears two *ortho*-substituted oxadiazoles. The net charges on the pyridine nitrogen atoms in these compounds (**2d–g**) obtained by semi-empirical (PM3) calculation[12] support this postulation (Table 1). The net-charge value for **2e** (−0.02) was less negative than those of the three other anologues, **2g** (−0.04), **2d** (−0.05) and **2f** (−0.08). Compound **2e** is, therefore, the weakest base of the four pyridine derivatives. Pyrimidine (pK_{a1} = 1.3[14]) is a weaker base than pyridine (pK_a = 5.23[14]) and the strong electron withdrawing oxadiazole units in **2h** reduce its basicity further. Therefore, **2h** is harder to protonate than its pyridine analogues (**2d–g**). However, the calculated N-charge densities of **2h** do not explain why **2h** could not be protonated.

The spectrum of the solution of protonated **2d** was the most complicated one among this series (Fig. 2). As was seen for **2g**, the new band at 380 nm caused by protonation could be attributed to a red shift of the $^1(\pi–\pi^*)$ transition, while the high-energy band at *ca.* 275 nm was the red shifted $^2(\pi–\pi^*)$ transition, which was not seen above 250 nm when the molecule was in the neutral solution. We assume that the band in the middle (~340 nm) is due to the non-protonated species. In other words, the absorption profile of the protonated **2d** is an overlap of the protonated and the neutral molecular absorptions. But this does not seem to be caused by an equilibrium existing between **2d** and the protonated **2d** species because this 340 nm band was not removed by prolonged bubbling of HCl gas through the solution or by adding methanesulfonic acid.

Acidification of **2g** solutions resulted in a much larger red shift than was seen for **2f**. PM3 Calculations of the protonated forms of **2d**, **2f** and **2g** show (Table 1) that protonated **2f** has a larger LUMO–HOMO band gap (6.10 eV) than those of **2d** (5.77 ev) and **2g** (5.78 eV). Therefore, a smaller red-shift of **2f** due to protonation should be expected. Apart from the reduced band gaps resulting from the protonation of **2d** and **2g**, a further red shift could also be derived from hydrogen-bonding induced co-planarisation,[13] which is not considered by the PM3 calculations.

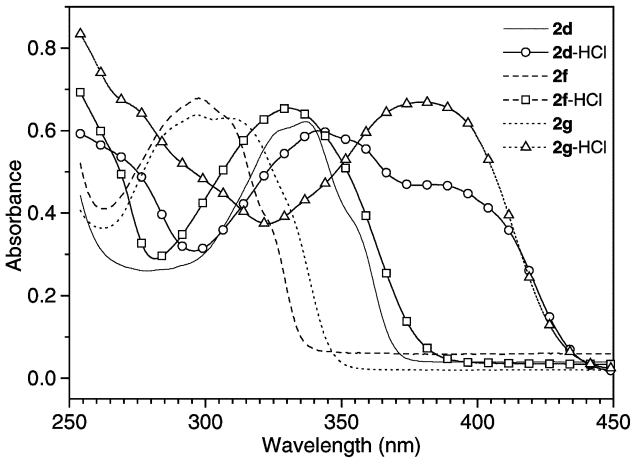

Fig. 2 UV-VIS absorption spectra of **2d**, **2f** and **2g** in chloroform with and without bubbling HCl gas through the solution.

Crystal structures

Compound **2c** crystallised from chloroform–toluene as a 1 : 1 toluene solvate. The asymmetric unit contains one molecule of **2c** (Fig. 3) and one toluene molecule. The latter is disordered between two partially overlapping positions with occupancies of *ca.* 2/3 and 1/3. Crystal **2g** contains no solvent, but the N atom of the central pyridine ring is disordered with equal probability between two positions, 1 and 5 (Fig. 3).

The conformation of molecule **2c** (or **2g**) can be described by dihedral angles (Table 2) between its five planar rings: the central benzene/pyridine (*i*), two oxadiazole (*ii* and *iv*) and two peripheral benzene (*iii* and *v*). The puckering is stronger than in **2a** and **2d**,[6] but still not sufficient to prevent conjugation. Both **2c** and **2g** have *syn* orientations of the two oxadiazole rings, in contrast with the *anti*-orientations in **2a** and **2d** molecules, which have crystallographic C_i symmetry.

The mean plane of molecule **2c** is nearly parallel to the

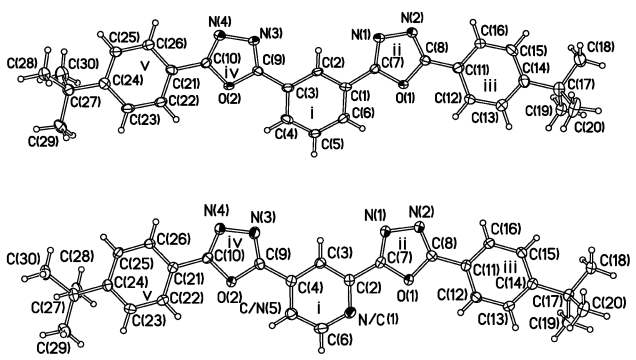

Fig. 3 Molecular structures of **2c** (top) and **2g**, showing 50% thermal ellipsoids, C/N disorder in the pyridine ring and the notation of the rings (*i* to *v*).

Table 2 Dihedral angles (°) between ring planes[a]

Planes	2c	2g	Planes	2c	2g
i/ii	17.4	8.7	i/iv	5.8	1.0
ii/iii	15.5	16.8	iv/v	7.8	21.1
i/iii	25.2	25.1	i/v	18.9	20.8
ii/iv	16.1	9.4	iii/v	10.4	14.3

[a]For ring notation see Fig. 3.

crystallographic (2 0 1) plane, and the long axis of the molecule to the [−2 0 1] vector. The mean plane of molecule **2g** is parallel to the (−2 0 1) plane and its long axis to the [2 0 1] vector. Thus, in both structures the molecules are perpendicular to the crystallographic glide planes. Consequently, mean planes of all molecules **2c** or **2g** in the crystals are parallel within 6°, and their long axes within 3° (**2c**) or 7° (**2g**). The packing motif of both **2c** and **2g** is that of discreet layers (Fig. 4), interspersed by layers of toluene molecules in **2c**. The surface of a layer consists of *t*-Bu groups, while the aromatic rings and the electronegative atoms are hidden inside the layers. Thus **2c** and **2g** satisfy two of Horowitz's conditions for a good thin-layer charge mobility:[15] layered packing and parallel orientation of all molecules. However, the structures do not comply well with the third condition: the long axes of the molecules must be close to normality with the maximum-density plane of the layer, or in other words, the longitudinal slip between molecules must be minimal. In fact, the slip amounts to *ca.* 6 Å in **2c** and 4 Å in **2g**, compared to the total length of the molecule of 26.5 Å. The long molecular axis is tilted from the perpendicular to the layer plane by *ca.* 60° in **2c** and 50° in **2g**. This latter rule, derived originally for oligothiophene derivatives, seems to be less universal for systems with more electronegative rings.[16]

LED fabrication and performance

Encouraged by the promising performance of PDPyDP (**2d**) in bilayer LEDs,[6,7] we have fabricated eight devices using ITO as the anode, rubrene-doped (20% by weight) MEH-PPV [MEH(Ru)] as the emissive material and Al as the cathode. These included a rubrene-doped MEH-PPV single-layer reference structure and seven bilayer devices of the general structure ITO/MEH(Ru)/compound **2**/Al. The aims of this work were: (1) to explore the ECHB behaviour of the materials by comparison with the reference LED; and (2) to relate the differences in the ECHB behaviour of the new compounds to their chemical structures. We, therefore, maintained the same thicknesses for the MEH(Ru), ECHB and Al layers in the different devices. The solids of materials **2b–h** were compressed, at 10 tons, into pellets using a die press of 13 mm diameter, and then broken into pieces prior to thermal evaporation.[17] The film thickness of the ECHB layers could be controlled to within ±20 nm during this process. The aluminium cathodes were evaporated directly on top of the ECHB layers using the same evaporation rate of 3.5 nm s^{-1} to 200 nm thick.

Fig. 5 shows the current density *versus* electric field relationships of the seven bilayer LEDs compared with the reference single layer device, while Fig. 6 gives the corresponding light output and electric field correlations. It is clear from these curves that the introduction of the oxadiazole-containing ECHB layers increases the electron-injection into the active MEH(Ru) layer in every bilayer case. Therefore, increased light outputs, hence higher external quantum efficiencies (EQEs) compared with the single layer reference, are observed. The electroluminescence (EL) of the bilayer LEDs had almost identical spectra to the single layer device, indicating that charge-combination and light emission took place exclusively within the MEH(Ru) layer. Fig. 7 shows the electroluminescence spectra of three bilayer LEDs using **2b**, **2d** and **2h** as the ECHB layers, and the spectrum of the reference single layer LED. The EL spectra of other bilayer LEDs are omitted for

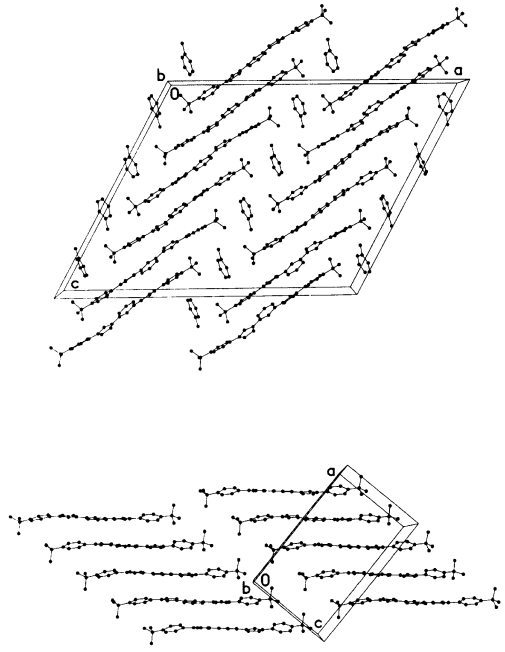

Fig. 4 Crystal packing in **2c** (top) and **2g**, projected on the (0 1 0) planes. Molecular layers are perpendicular to these planes.

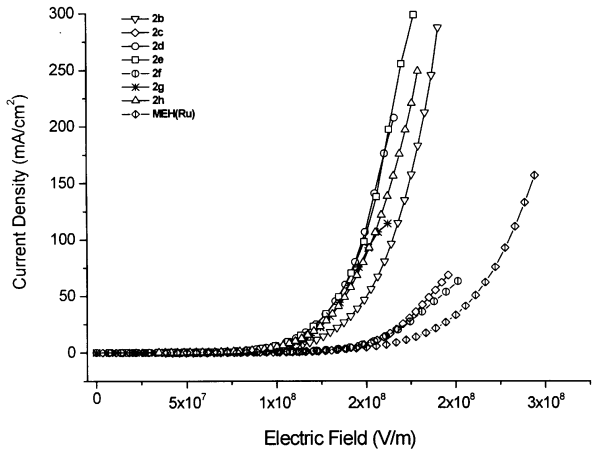

Fig. 5 Current density *versus* electric field characteristics for a single layer LED ITO/MEH-PPV(Ru)/Al and bilayer LEDs ITO/MEH-PPV(Ru)/**2**/Al. The thicknesses of MEH-PPV(Ru) were uniformally 90 nm in all cases.

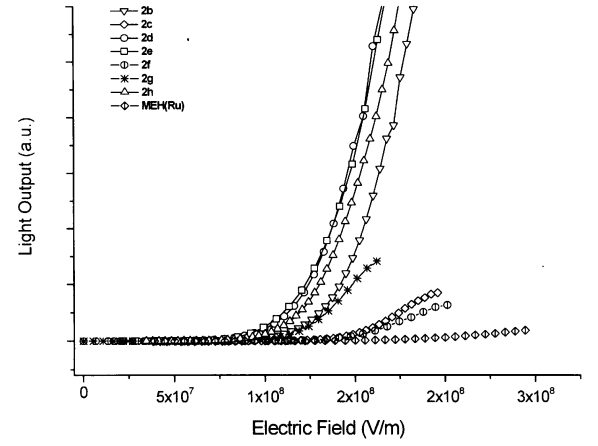

Fig. 6 Light out *versus* field characteristics for the same devices described in Fig. 5.

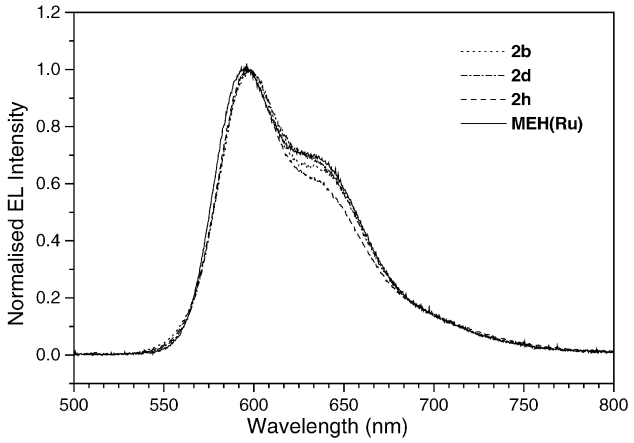

Fig. 7 Normalised electroluminescence spectra of a single layer LED and bilayer LEDs using **2b**, **2d** and **2h** as the ECHB layer, correspondingly. The device configurations are described in Fig. 5.

clarity. These have essentially identical profiles showing a peak at 590 nm and a shoulder at *ca* 630 nm, coincident with the EL emission of a single layer MEH-PPV device.

Fig. 8 shows the EQEs of the LEDs with and without compounds **2** as ECHB layers *versus* current densities. In the bilayer devices, compounds **2** improved the EQE of the rubrene doped MEH-PPV by a factor of 5 to 20 times at a current density of 40 mA cm^{-2}. The EQE values of the LEDs with each particular compound are listed in Table 1. The EQE of the reference ITO/MEH(Ru)/Al device was 0.007% under the same conditions. At current densities lower than 40 mA cm^{-2}, the EQE of PDPyDP (**2d**), the first derivative of this series which we had synthesised, came second after its angular isomer PDPy-2,6 (**2e**). At higher current densities, the EQEs of these two materials both reached *ca*. 0.14%. The pyrimidine analogue (**2h**) had an EQE comparable to the linear phenylene analogue (**2b**) over almost the whole operating range of current density. But the EQE of **2h** was lower than those of **2d** and **2e**. This is reminiscent of our recent report[4e] that no further improvement in device performance for a bilayer LED with a spun ECHB layer was observed when pyridine units were used to replace the benzene units in polymeric PBD [PBD = 2-(4-biphenylyl)-5-phenyl-1,3,4-oxadiazole]. Similarly, Galvin and co-workers found that a higher proportion of oxadiazole units incorporated into the polymer chain of PPV did not further increase the EQE of its single layer device.[4b] The other three angular derivatives resulted in lower EQE increases compared with the single layer MEH(Ru) reference. These included OXD-7 (**2c**) (8 fold increase), PDPy-2,4 (**2g**) (7 fold increase) and PDPy-3,5 (**2f**) (5 fold increase) (Table 1). It is

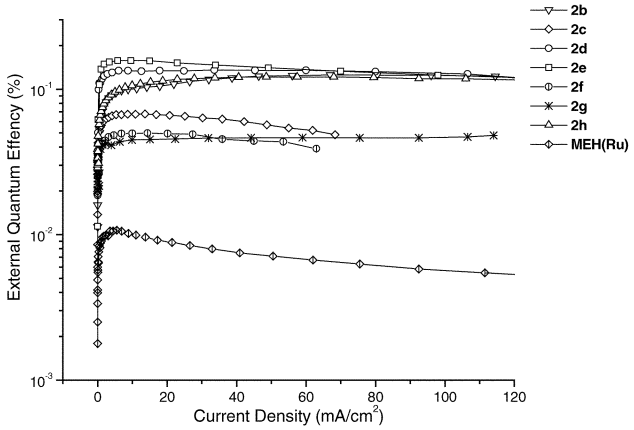

Fig. 8 External quantum efficiency *versus* current density relationships for the same single and bilayer LEDs described in Fig. 5.

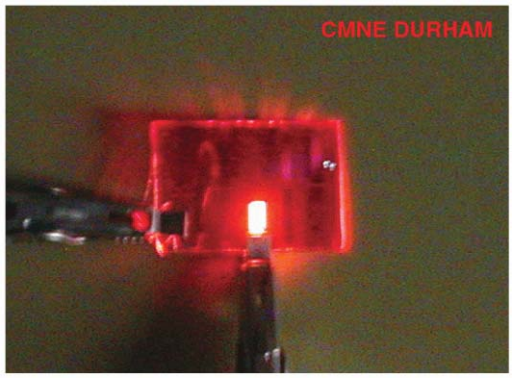

Fig. 9 A photograph of a bilayer LED ITO/MEH-PPV(Ru) (90 nm)/PDPyDP(55 nm)/Al working at a current density of *ca.* 100 mA cm^{-2} under forward bias, without encapsulation. The shadows of the aluminium electrodes of the other LEDs on the same substrate are seen projected onto the surface of a lab-bench. The peak external quantum efficiency of the LED was *ca*. 0.7% and the brightness was *ca.* 4,000 Cd m^{-2}.

worth pointing out that the EQE values quoted in this work are not the maximum EQEs we can achieve for this series of materials. More efficient LEDs can be fabricated by optimising both the MEH(Ru) and ECHB layers. An EQE of 0.7% has been achieved by a ITO/MEH(Ru)(90 nm)/**2d** (55 nm)/Al structure. The photograph of this LED is shown as Fig. 9. Notably, a considerable amount of emitted light, which was wave-guided to the glass edge due to refraction inside the glass substrate, was not counted for the EQE calculation in our measurements. The lost fraction of the light can be seen from the glowing edges of the glass substrate in Fig. 9.

Comparison with the PM3 calculated LUMO levels (Table 1) indicates that there is no clear correlation between those values and the experimental EQEs. Earlier, Jenekhe and co-workers found that variation of the LUMO energy levels by *ca*. 0.5 eV among a series of polyquinolines did not directly influence either the turn-on electric field or EL efficiency.[18] To explain this, several possible reasons need to be considered. As the EQE depends on many experimental variables, *e.g.*, film thickness, morphology of the materials, interface behaviour *etc.*, variation of any of these variables will influence the EQE of a device. This effect, arising from configuration factors, could be more pronounced than that caused by a LUMO energy level variation. In addition, some film properties, such as morphology of a material, are intrinsic to the molecules, which could hardly be controlled by evaporation. An unfavourable film to charge injection/transport can lead to inefficient LED regardless of how favourable the LUMO level is. We have proved that, in spite of the very similar molecular structures, compounds **2b–h** have different crystallinity (*vide supra* for the X-ray structures of **2c** and **2g**; see reference 6 for the X-ray structures of **2a** and **2d**) and sublimation temperatures. Although evaporated films and single crystals are not directly comparable, different crystallinity could still imply a difference in film properties and, consequently, a difference in device performances. Further extensive study on **2e** and **2h**, which showed performances comparable with **2d**, are under way in our laboratories.

Conclusions

Three new pyridine analogues, **2e**, **2f** and **2g**, of the well known electron-injecting/hole blocking material OXD-7 (**2c**) and one pyrimidine analogue (**2h**) of PDPyDP[6,7] have been synthesised. The X-ray crystal structures of **2c** and **2g** have been determined, and compared with those of **2a** and **2d**. Bilayer LEDs using ITO as the anode, rubrene-doped (20% by weight) MEH-PPV as the emissive material, **2b–h** as the electron-injecting

material and aluminium as the cathode have been fabricated. Among these new materials, **2e** and **2h** have proved to be comparable to the efficient electron-injecting material PDPyDP (**2d**), and to be more efficient than the well-known OXD-7. LUMO levels of these molecules have been calculated by the PM3 method. However, no obvious correlation between these levels and the EQEs of the bilayer LEDs using these materials as the ECHB layers were observed.

Experimental

General. Elemental analyses were obtained on a Carlo-Erba Strumentazione instrument. Melting points were determined in open-end capillaries using a Stuart Scientific melting point apparatus SMP3 at a ramp rate of 2.5 °C min^{-1} without calibration. Solution ^1H NMR and ^{13}C NMR spectra were recorded with a Varian Unity 300 spectrometer at frequencies of 299.91 and 75.41 MHz, respectively, and chemical shifts are reported in ppm downfield of TMS. Mass spectra were obtained on a VG7070E instrument operating in EI mode at 70 eV. UV-VIS absorption spectra were recorded on a Unicam UV2 spectrometer.

Synthesis of materials. MEH-PPV was synthesized based on the patented method.[19] The number-average molecular weight was found to be 55,400 by GPC using polystyrene as standard in chloroform solution. Basic chemicals were purchased from Aldrich and Lancaster and were used without further purification unless elsewhere indicated. Pyridine was dried over NaOH pellets for three days and used without distillation. THF was freshly distilled under argon over potassium metal. Methanol and ethanol were dried by refluxing over Mg turnings, then distilled under argon immediately before use.

X-Ray crystallography. X-Ray diffraction experiments were carried out on a SMART 3-circle diffractometer with a 1K CCD area detector, using graphite-monochromated Mo-$K\alpha$ radiation ($\bar{\lambda} = 0.71073$ Å) and a Cryostream (Oxford Cryosystems) open-flow N_2 gas cryostat. A hemisphere (**2c**) or full sphere (**2g**) of reciprocal space was covered by a combination of 4 or 5 sets of ω scans; each set at different φ and/or 2θ angles. The structures were solved by direct methods and refined by full-matrix least squares against F^2 of all data, using SHELXTL software.[20] Crystal data and experimental details are summarised in Table 3. CCDC 171139 (**2c**) and 171140 (**2g**). See http://www.rsc.org/suppdata/jm/b1/b106907c/ for crystallographic files in .cif or other electronic format.

Device fabrication. ITO-coated glass used as the anode was first patterned and etched into strips of 2 mm width. It was then cleaned by ultrasonication in soap, deionised water, acetone and isopropyl alcohol sequentially, and dried with a pressure nitrogen gun. Rubrene doped (20% by weight) MEH-PPV, which was used as the active material, was spin-coated on the ITO coated glass from its solution in a 1 : 1 mixture of chloroform and *p*-xylene to form a film of dry thickness *ca.* 90 nm, for both single layer and double layer devices. The second layer (≈60–70 nm) of electron-injecting/hole-blocking material was deposited by vacuum evaporation at pressures of *ca.* 6×10^{-6} mbar and evaporation rate of 0.1–0.2 nm s^{-1}. Finally, an Al cathode was evaporated under similar conditions in strips of 1 mm width normal to the ITO strips. In this work, the relative thicknesses of both the emissive and electron-injection layers were not optimised for maximum brightness and efficiencies. All electrical measurements were undertaken in a vacuum chamber (*ca.* 10^{-1} mbar). Biases were supplied by a Keithley 2400 source using a linear staircase step of 0.5 V with a 1 s delay between measurements. The EL devices were mounted over a large area silicon photodiode. Not all the light from the LED (*i.e.* scattered light) was collected by the photodiode and so the efficiencies quoted in this paper are lower limits. The photocurrents generated were recorded using a Keithley 485 digital picoammeter. For quantum efficiency measurements, the light power was calculated with a typical conversion factor of 0.32 A W^{-1} at 590 nm corresponding to the electroluminescence peak of MEH-PPV. Film thicknesses were measured with an Alpha-step 200 stylus profilometer.

Table 3 Crystal data and experimental details

Compound	**2c**	**2g**
Formula	$C_{30}H_{30}N_4O_2 \cdot C_7H_8$	$C_{29}H_{29}N_5O_2$
Formula weight	570.71	479.57
T/K	100	100
Symmetry	Monoclinic	Monoclinic
Space group	*C*2/*c* (# 15)	$P2_1/c$ (# 14)
a/Å	36.596(4)	18.7544(12)
b/Å	6.445(1)	11.6181(7)
c/Å	29.798(3)	11.4838(7)
β/°	118.10(1)	90.221(4)
V/Å^3	6199.8(13)	2502.2(3)
Z	8	4
Refls collected	17344	27560
Unique refls	5465	5747
R_{int}	0.177	0.061
Refls $F^2 > 2\sigma(F^2)$	3261	4388
$R[F^2 > 2\sigma(F^2)]$	0.087	0.047
w$R(F^2)$, all data	0.213	0.118

1,3-Bis[2-(4-*tert*-butylphenyl)-1,3,4-oxadiazol-5-yl]benzene (2c/OXD-7). By analogy to the synthesis of PDVDP (**2a**),[6,21] compound **2c** was synthesized from isophthalic dihydrazide (10 mmol) reacting with *tert*-butylbenzoyl chloride (22 mmol) in 1 : 1 (v/v) pyridine–DMF (40 cm^3, dried) mixture. The white solid of the bishydrazine (**1c**) obtained was then treated with refluxing $POCl_3$. The crude product was then chromatographed on silica (eluent: ethyl acetate–dichloromethane 1 : 3 v/v) to afford pure OXD-7 in 65% yield (for two steps) as white crystals, mp: 238.4–239.7 °C (Calcd for $C_{30}H_{30}N_4O_2$: C, 75.29; H, 6.32; N, 11.71. Found: C, 74.88; H, 6.19; N, 11.76%). $\delta_H(CDCl_3)$ 1.39 (s, 18H), 7.59 (m, 4H), 7.73 (t, $J_{AB} = 7.8$ Hz, 1H), 8.12 (m, 4H), 8.34 (dd, $J_{AB} = 7.8$ Hz, $J_{AC} = 1.8$ Hz, 2H), 8.87 (t, $J = 1.5$ Hz, 1H). δ_C ($CDCl_3$) 31.11, 35.13, 120.76, 124.89, 125.11, 126.11, 126.90, 129.64, 129.96, 155.64, 163.40, 165.11. *m*/*z*: 478 (M^+, 74), 463 ($M^+ - 15$, 100). The NMR data were in agreement with the literature, although no mp, mass spectrum and microanalysis were given therein.[22] Slow evaporation of a solution of **2c** in a chloroform–toluene mixture afforded white plates, suitable for X-ray analysis.

2,6-Bis[2-(4-*tert*-butylphenyl)-1,3,4-oxadiazol-5-yl]pyridine (2e/PDPy-2,6). Pyridine-2,6-dicarboxylic acid dihydrazide was prepared by refluxing the dimethyl ester with hydrazine monohydrate in ethanol, in 98% yield, as a white solid, mp: 285.4–287.6 °C (280 °C,[23a] 307 °C[23b])

The dihydrazide (1.95 g, 10 mmol) was suspended in dry THF (40 cm^3), followed by addition of pyridine (10 cm^3). 4-(*tert*-Butyl)benzoyl chloride (4.3 g, 22 mmol) was added dropwise at 30 °C with stirring. The mixture was then stirred and refluxed for 1 h, then cooled to rt to yield a white slurry. Water (200 cm^3) was added slowly with stirring, then the mixture was suction filtered. The filter cake was boiled in water (*ca.* 200 cm^3), suction filtered while hot, washed with hot water, then dried to yield a white powder of compound **1e** 5.05 g (98%). δ_H (DMSO-d_6) 1.29 (s, 18H), 7.54 (d *J* 8.4, 4H), 7.88 (d, *J* 8.4, 4H), 8.29 (m, 3H), 10.59 (s, 2H), 11.25 (s, 2H). δ_C (DMSO-d_6) 30.94, 34.75, 125.18, 125.38, 127.36, 129.71, 140.03, 147.85, 154.86, 162.31, 165.82. The product was insoluble in most organic solvents. While in solvents that could dissolve it when hot, *e.g.* ethanol, a gel formed. Therefore, the

precursor compound was directly used for the following cyclisation without further purification.

Compound **1e** (5.05 g, 9.79 mmol) was mixed with $POCl_3$ (30 cm^3) and the mixture was stirred under reflux for 2 h to afford a clear yellow solution. The excess $POCl_3$ was removed by vacuum distillation to give a pale-yellow slurry. Ice-water (*ca.* 100 cm^3) was added and the solid which formed after standing was collected by suction filtration, then washed with a large volume of water, dilute Na_2CO_3 solution and water, subsequently. The dry solid was dissolved in dichloromethane (DCM) then purified by column chromatography (silica, eluent: DCM–ethyl acetate 2 : 1 v/v) and crystallisation (chloroform–ethyl acetate) to yield a white solid of compound **2e** (PDPy-2,6) with a pearl-like appearance, 3.91 g (83%, 81% for the last two steps), mp 302.6–303.8 °C (Calcd. for $C_{29}H_{29}N_5O_2$: C, 72.63; H, 6.10; N, 14.60. Found: C, 72.26; H, 6.01; N, 14.62%); *m*/*z* (%): 479 (M^+, 56), 464 ($M^+ - 15$, 100); δ_H ($CDCl_3$) 1.40 (s, 18H), 7.60 (d *J* 8.4, 4H), 8.12 (t, *J* 8.0, 1H), 8.20 (d, *J* 8.4, 4H), 8.48 (d, *J* 7.8, 2H). δ_C ($CDCl_3$) 31.12, 35.17, 120.61, 124.99, 126.09, 127.27, 138.46, 144.33, 155.86, 163.02, 166.05.

3,5-Bis[2-(4-*tert*-butylphenyl)-1,3,4-oxadiazol-5-yl]pyridine (2f/PDPy-3,5). Pyridine-3,5-dicarboxylic acid (5.01 g, 30 mmol) was refluxed in $SOCl_2$ (30 cm^3) for 8 h to obtain a clear yellow solution. The excess thionyl chloride was removed by distillation to yield a yellow solid residue. Dry methanol (50 cm^3) was added to the solid and the mixture was refluxed for 10 min followed by an addition of pyridine (10 cm^3) dropwise. The solution was further stirred for 0.5 h at rt. Water (100 cm^3) was added to the hot solution which was then cooled to rt. Pale-yellow needles of dimethyl pyridine-3,5-dicarboxylate were obtained by suction filtration and washing with cold 1 : 1 methanol–H_2O, in a yield of 4.38 g (75%), mp 86.7–87.8 °C (84–85 °C[24]). δ_H ($CDCl_3$) 3.96 (s, 6H), 8.36 (t, *J* 2.1, 1H), 9.33 (s, 2H); δ_C ($CDCl_3$) 52.65, 125.89, 137.94, 154.12, 164.80.

Similar to its 2,6-isomer, pyridine-3,5-dicarboxylic acid dihydrazide was synthesised in 99% yield as a light yellow solid, mp 232.8–234.6 °C (decomp.) (238–240 °C[25]); δ_H (DMSO-d_6) 4.63 (s, br, 4H), 8.55 (s, 1H), 9.06 (s, 2H), 10.05 (s, br, 2H); δ_C (DMSO-d_6) 128.76, 133.66, 149.90, 163.75.

By analogy to the synthesis of compound **1e**, compound **1f** was synthesised as a white solid in 85% yield, using pyridine as solvent, mp 283.4–284.9 °C, *m*/*z* (%): 497 ($M^+ - 18$, 4), 479 ($M^+ - 136$, 24), 464 (61), 161 (100); δ_H (DMSO-d_6) 1.30 (s, 18H), 7.52 (d *J* 8.2, 4H), 7.83 (d, *J* 8.2, 4H), 8.72 (s, 1H), 9.15 (s, 2H), 10.67 (s, 4H). δ_C (DMSO-d_6) 30.96, 34.66, 125.32, 127.07, 129.88, 130.58, 133.75, 150.02, 154.28, 163.43, 163.93. The solid was directly used for the following reaction without further purification.

Similarly to compound **2e**, PDPy-3,5 (**2f**) was obtained as white crystals, in 73% yield, mp 291.8–292.2 °C (Calcd. for $C_{29}H_{29}N_5O_2$: C, 72.63; H, 6.10; N, 14.60. Found: C, 72.20; H, 6.03; N, 14.66%); *m*/*z* (%): 479 (M^+, 42), 464 ($M^+ - 15$, 100); δ_H ($CDCl_3$) 1.38 (s, 18H), 7.59 (d *J* 8.4, 4H), 8.11 (d, *J* 8.4, 4H), 9.10 (t, *J* 2.1, 1H), 9.51 (d, *J* 2.1, 2H). δ_C ($CDCl_3$) 31.09, 35.17, 120.35, 120.91, 126.22, 127.02, 131.57, 149.80, 156.05, 161.38, 165.59.

2,4-Bis[2-(4-*tert*-butylphenyl)-1,3,4-oxadiazol-5-yl]pyridine (2g/PDPy-2,4). The diethyl ester of 2,4-pyridinedicarboxylic acid was synthesized by refluxing the diacid monohydrate with ethanol[23*a*] in the presence of H_2SO_4. The diester was then treated with hydrazine monohydrate in ethanol to yield the corresponding dihydrazide as an off-white solid, mp 258–260 °C (257 °C[26]). δ_H (DMSO-d_6) 4.64 (s, 4H), 7.89(dd, J_{AB} 5.1, J_{AC} 1.8, 1H), 8.33 (d, J_{AC} 0.9, 1H), 8.71 (dd, J_{AB} 5.5, J_{AC} 0.6, 1H), 9.98 (s, 1H), 10.27 (s, 1H); δ_C (DMSO-d_6) 119.10, 123.27, 141.74, 149.26, 150.63, 162.14, 163.23.

By analogy to the synthesis of compound **1e**, compound **1g** was synthesised as a white solid in 99% yield, using pyridine as solvent. The crude product was directly cyclised with $POCl_3$ into compound **2g** without purification. Chromatography (silica, eluent: DCM–ethyl acetate 3 : 1 v/v) and recrystallisation from a DCM–ethanol mixture yielded pale-yellow prisms of **2g** (46%), mp 216.3–217.6 °C (Calcd. for $C_{29}H_{29}N_5O_2$: C, 72.63; H, 6.10; N, 14.60. Found: C, 72.08; H, 6.05; N, 14.43%). A single crystal for X-ray analysis was prepared by slow evaporation of a chloroform–ethanol solution. *m*/*z* (%): 479 (M^+, 38), 464 ($M^+ - 15$, 100); δ_H ($CDCl_3$) 1.386 (s, 9H), 1.394 (s, 1H), 7.58 (d, *J* 7.5, 2H), 7.60 (d, *J* 7.5, 2H), 8.13 (d, *J* 8.5, 2H), 8.20 (d, *J* 8.5, 2H), 8.21 (dd, J_{AB} 5.1, J_{AC} 1.8, 1H), 8.94 (m, 1H), 9.02 (d, *J* 5.5, 1H). δ_C ($CDCl_3$) 31.06, 31.07, 119.50, 120.20, 120.47, 122.00, 126.07, 126.24, 127.11, 127.19, 132.57, 144.91, 151.27, 155.92, 156.25, 161.76, 163.05, 165.94, 165.99.

2,5-Bis(3-hydroxy-3-methylbut-1-ynyl)pyrimidine (3). 2,5-Dibromopyrimidine[9] (7.82 g, 32.87 mmol), 2-methylbut-3-yn-2-ol (8.4 g, 100 mmol), CuI (250 mg), $Pd(PPh_3)_2Cl_2$ (500 mg), and triethylamine (30 cm^3) were mixed in dry THF (150 cm^3), and stirred at rt for 1 h then refluxed for an additional 1 h to obtain a brown suspension. The hot mixture was filtered under gentle suction through a Celite pad which was washed with diethyl ether. The solvent from the brownish filtrate was evaporated under vacuum to leave a solid residue which was recrystallised from toluene to yield compound **3** (6.80 g, 85%) as off-white plates, mp 175.8–176.8 °C (Calcd. for $C_{14}H_{16}N_2O_2$: C, 68.83; H, 6.60; N, 11.47. Found: C, 68.76; H, 6.59; N, 11.55%). *m*/*z* (%): 244 (M^+, 22), 229 (100), 201 (43), 171 (78); δ_H (DMSO-d_6) 1.46 (s, 12H), 5.63 (s, 1H), 5.70 (s, 1H), 8.78 (s, 2H); δ_C (DMSO-d_6) 30.98, 31.20, 63.51, 63.78, 79.89, 95.64, 104.16, 117.29, 149.65, 158.94.

Diethyl 2,5-pyrimidinedicarboxylate (5). Compound **3** (4.13 g, 16.91 mmol) was suspended in water (150 cm^3). Aliquat-336[10] (*ca.* 0.5 g) was added and the mixture was heated to boiling with stirring. $KMnO_4$ powder (15.5 g) was added in small portions until the purple colour remained stable. The heating and stirring were continued for an additional 2 h. The hot mixture was suction filtered and the brown MnO_2 filter cake was washed 3 times with hot water. The volume of the filtrate was reduced by vacuum evaporation to *ca.* 30–50 cm^3, followed by a slow addition of 48% HBr into the residue until its pH was *ca.* 5. A white solid of 2,5-pyrimidinedicarboxylic acid (**4**) was obtained by suction filtration and washing with water and ethanol. The diacid was too insoluble in organic solvents to allow solution spectral measurements and it did not melt below 330 °C. *m*/*z* (EI, %): 168 (M^+, 5), 151 (2), 124 (100), 97 (6). The dry diacid was refluxed in thionyl chloride (20 cm^3) for 4 h to yield a clear pale-yellow solution. The remaining $SOCl_2$ was removed by distillation then by vacuum evaporation. Dry ethanol (50 cm^3) was added to the solid residue and the mixture was refluxed for 1 h. Pyridine (10 cm^3) was added and the solution was refluxed for an additional 2 h. Ethanol was removed by vacuum evaporation then water (*ca.* 50 cm^3) was added. The pH of the aqueous phase was brought to *ca.* 9 using 5% Na_2CO_3 solution and the mixture was extracted with diethyl ether (4 × 20 cm^3). The solution was dried over $MgSO_4$ then filtered through a silica pad. The solid from the filtrate was crystallised from petroleum ether (bp 40–60 °C) to afford diester **5** as white needles (2.66 g, 70% for both steps), mp: 67.2–68.5 °C (Calcd. for $C_{10}H_{12}N_2O_4$: C, 53.57; H, 5.39; N, 12.49. Found: C, 53.54; H, 5.42; N, 12.51%). *m*/*z* (%): 224 (M^+, 5), 179 (39), 152 (100), 124 (25), 107 (11), 79 (12). δ_H ($CDCl_3$) 1.42 (m, 6H), 4.45 (q, *J* 6.9, 2H), 4.54 (q, *J* 7.2, 2H), 9.40 (s, 2H). δ_C ($CDCl_3$) 14.17, 62.44, 63.19, 125.42, 158.61, 158.83, 162.66, 162.71.

2,5-Pyrimidinedicarboxylic acid dihydrazide (6). Similar to the pyridine analogues, by treating the diester **5** with hydrazine

monohydrate in ethanol, the dihydrazide **6** was obtained as a yellow solid in 98% yield, mp 240.8 °C (decomp.), (Calcd. for $C_6H_8N_6O_2$: C, 36.74; H, 4.11; N, 42.84. Found: C, 36.73; H, 4.10; N, 43.14%). *m*/*z* (%): 196 (M^+, 57), 165 (38), 137 (100), 106 (14), 79 (26), 53 (38). δ_H (DMSO-d_6) 4.68 (s, 4H), 9.21 (s, 2H), 10.22 (s, 2H). δ_C (DMSO-d_6) 127.17, 156.05, 159.18, 160.69, 161.73.

Compound 1h. Following the same procedure for the pyridine analogues, using pyridine as solvent, compound **1h** was prepared from the dihydrazide **6** and *tert*-butylbenzoyl chloride in 43% yield. The compound formed a complex with DMSO, when crystallised from hot DMSO-H_2O mixture (insoluble in pure DMSO), as white needles, mp 280.3–280.8 °C (Calcd. for $C_{28}H_{32}N_6O_4$-C_2H_6OS: C, 60.59; H, 6.44; N, 14.13. Found: C, 60.51; H, 6.42; N, 14.30). *m*/*z* (%): 516 (M^+, 3), 498 (5), 480 (7), 465 (14), 308 (5), 161 (100), 108 (29), 63 (38). δ_H (DMSO-d_6) 1.31 (s, 18H), 7.54 (d, *J* 8.2, 2H), 7.56 (d, *J* 8.4, 2H), 7.89 (d, *J* 8.2, 4H), 9.42 (s, 2H), 10.60 (s, 1H), 10.69 (s, 1H), 10.96 (s, 1H), 11.08 (s, 1H). δ_C (DMSO-d_6) 31.62, 35.41, 35.43, 125.97, 126.07, 127.83, 128.10, 130.13, 130.34, 155.47, 155.66, 157.49, 159.79, 161.91, 162.81, 165.95, 166.35.

2,5-Bis[2-(4-*tert*-butylphenyl)-1,3,4-oxadiazol-5-yl]pyrimidine (2h/PDPmDP). Similar to its pyridine analogues, treating compound **1h** (2.49 g, 4.82 mmol) with $POCl_3$ (20 cm^3) gave the crude product of compound **2h**, which was chromatographed (silica, eluent: DCM–Et_2O 2 : 1 v/v), then crystallised from DCM–ethanol to afford off-white hairy needles (1.65 g, 71%), mp 288.1–289.1 °C (Calcd. for $C_{28}H_{28}N_6O_2$: C, 69.98; H, 5.87; N, 17.49. Found: C, 69.44; H, 5.83; N, 17.44%). *m*/*z* (%): 480 (M^+, 50), 465 ($M^+ - 15$, 100), 290 (11), 225 (13), 161 (8), 145 (16). δ_H ($CDCl_3$) 1.358 (s, 9H), 1.361 (s, 9H), 7.55 (d, *J* 8.0, 2H), 7.58 (d, *J* 8.1, 2H), 8.08 (d, *J* 8.4, 2H), 8.17 (d, *J* 8.4, 2H), 9.625 (s, 2H). δ_C ($CDCl_3$) 31.03, 35.17, 119.33, 119.94, 120.19, 126.13, 126.26, 127.11, 127.36, 154.25, 155.55, 156.30, 156.39, 159.36, 162.01, 165.92, 166.55.

Acknowledgements

We thank Professor J. A. K. Howard for the use of X-ray facilities, and EPSRC for funding the improvement of X-ray instrumentation.

References

1 (*a*) Reviews A. Kraft, A. C. Grimsdale and A. B. Holmes, *Angew. Chem., Int. Ed.*, 1998, **37**, 402; (*b*) J. L. Segura, *Acta Polym.*, 1998, **49**, 319; (*c*) R. H. Friend, R. W. Gymer, A. B. Holmes, J. H. Burroughes, R. N. Marks, C. Taliani, D. D. C. Bradley, D. A. Dos Santos, J. L. Brédas, M. Lögdlund and W. R. Salenek, *Nature*, 1999, **397**, 121; (*d*) U. Mitschke and P. Bäuerle, *J. Mater. Chem.*, 2000, **10**, 1471.
2 (*a*) Reviews B. Schultz, M. Bruma and L. Brehmer, *Adv. Mater.*, 1997, **9**, 601; (*b*) M. Thelakkat and H.-W. Schmidt, *Polym. Adv. Technol.*, 1998, **9**, 429.
3 (*a*) C. Adachi, S. Tokito, T. Tsutsui and S. Saito, *Jpn. J. Appl. Phys.*, 1988, **27**, L713; (*b*) Y. Hamada, C. Adachi, T. Tsutsui and S. Saito, *Jpn. J. Appl. Phys.*, 1992, **31**, 1812; (*c*) Y. Shirota, *J. Mater. Chem.*, 2000, **10**, 1.
4 (*a*) X.-C. Li, F. Cacialli, M. Giles, J. Grüner, R. H. Friend, A. B. Holmes, S. C. Moratti and T. M. Yong, *Adv. Mater.*, 1995, **7**, 898; (*b*) Z. Peng, Z. Bao and M. E. Galvin, *Chem. Mater.*, 1998, **10**, 2086; (*c*) Z.-K. Chen, H. Meng, Y.-H. Lai and W. Huang, *Macromolecules*, 1999, **32**, 4351; (*d*) Z. Peng and J. Zhang, *Chem. Mater.*, 1999, **11**, 1138; (*e*) C. Wang, M. Kilitziraki, L.-O. Palsson, M. R. Bryce, A. P. Monkman and I. D. W. Samuel, *Adv. Funct. Mater.*, 2001, **11**, 47.
5 (*a*) C. Wang, M. Kilitziraki, J. A. H. MacBride, M. R. Bryce, L. Horsburgh, A. Sheridan, A. P. Monkman and I. D. W. Samuel, *Adv. Mater.*, 2000, **12**, 217; (*b*) J. K. Kim, J. W. Yu, J. M. Hong, H. N. Cho, D. Y. Kim and C. Y. Kim, *J. Mater. Chem.*, 1999, **9**, 2165.
6 C. Wang, G.-Y. Jung, Y. Hua, C. Pearson, M. R. Bryce, M. C. Petty, A. S. Batsanov, A. E. Goeta and J. A. K. Howard, *Chem. Mater.*, 2001, **13**, 1167.
7 (*a*) G.-Y. Jung, C. Wang, C. Pearson, M. R. Bryce, I. D. W. Samuel and M. C. Petty, *Proceedings of the 45th SPIE Annual Meeting*, San Diego, 2000, **4105**, 307; (*b*) G. Y. Jung, C. Wang, P. Cea, C. Pearson, M. R. Bryce and M. C. Petty, submitted.
8 G.-Y. Jung, *Ph.D. Thesis*, University of Durham, 2001.
9 (*a*) The compound was synthesised in a multi-step sequence, from 2-hydropyrimidine hydrochloride based on the following literature: B. W. Arantz and D. J. Brown, *J. Chem. Soc.*, 1971, 1889; (*b*) D. J. Brown and J. M. Lyall, *Aust. J. Chem.*, 1964, **17**, 794; (*c*) H. Schlosser and R. Wingen, US Pat., 5,371,224 (1994). However, we modified this tedious procedure and the details will be published elsewhere.
10 P.-M. Windscheif and F. Vögtle, *Synthesis*, 1994, 87.
11 (*a*) Pyrimidinedicarboxylic acid from oxidation of 2-methylquinazoline: M. Radojkovic-Velickovic and M. Misic-Vukovic, *J. Serb. Chem. Soc.*, 1989, **54**, 563; (*b*) *Chem. Abstr.* 1991, **114**, 101895y.
12 HyperChem, Version 5.02, Hypercube, Inc., 1997. All calculations listed in Table 1 terminated at the RMS gradient of 0.01 kcal Å mol^{-1}.
13 A. P. Monkman, L.-O. Pålsson, R. W. T. Higgins, C. Wang, M. R. Bryce, A. S. Batsanov and J. A. K. Howard, submitted.
14 R. M. Acheson, *An Introduction to the Chemistry of Heterocyclic Compounds*, 3rd ed., John Wiley & Sons, 1976, New York, pp 397.
15 (*a*) G. Horowitz, *Adv. Mater.*, 1998, **10**, 365; (*b*) G. Horowitz, *J. Mater. Chem.*, 1999, **9**, 2021.
16 U. Mitschke, E. M. Osteritz, T. Debaerdemaeker, M. Sokolowski and P. Bäuerle, *Chem. Eur. J.*, 1998, **4**, 2211.
17 M. Kilitziraki, A. J. Moore, M. C. Petty and M. R. Bryce, *Thin Solid Films*, 1998, **335**, 209.
18 X. Zhang, A. S. Shetty and S. A. Jenekhe, *Macromolecules*, 1999, **32**, 7422.
19 A. J. Heeger and D. Braun, US Pat. 5408019 (1995).
20 *SHELXTL*, Version 5.10, Bruker AXS Inc., Madison, Wisconsin, USA, 1997.
21 (*a*) J. Pan, C. Wang and Z. Gao, *Gaodeng Xuexiao Huaxue Xuebao*, 1988, **9**, 41; (*b*) *Chem. Abstr.*, 1989, **110**, 75399k.
22 A. Kraft, *Leibigs Ann./Recueil*, 1997, 1463.
23 (*a*) O. Efimovsky and P. Rumpf, *Bull. Soc. Chim. Fr.*, 1954, 648; (*b*) V. B. Rana and M. P. Teotia, *Indian J. Chem., Sect. A*, 1980, **19**(3), 267.
24 V. E. Blokhin, Z. Yu. Kokoshko, E. P. Dartsento and Z. V. Pushkareva, *J. Gen. Chem. USSR (Engl. Transl.)*, 1969, **39**, 1592.
25 G. B. Barlin, *Aust. J. Chem.*, 1985, **38**(10), 1491.
26 (*a*) T. Itai and M. Sekiyima, *Eisei Shikenjo Hokoku*, 1956, **74**, 115; (*b*) *Chem. Abstr.* 1957, **51**, 8740d.